Journal of Civil Engineering and Urban Planning (2025)
Clausius Scientific Press, Canada

DOI: 10.23977/jceup.2025.070307
ISSN 2616-3969 Vol. 7 Num. 3

Abnormal Location Method of Underground Petroleum Storage Cavern Based on Seepage Simulation

Yanan Zhao[1,2,*]

[1]*Power China, Zhongnan Engineering Corporation Limited, Changsha, 410014, Hunan, China*
[2]*Hunan Provincial Key Laboratory of Key Technology on Hydropower Development, Changsha, 410014, Hunan Province, China*
[*]*Corresponding author: izolt@163.com*

Keywords: Seepage Simulation; Fracture Network Model; Anomaly Location; Water Chemistry Analysis

Abstract: Underground water-sealed caverns are core facilities for China's strategic petroleum reserves. The accuracy of leak anomaly location directly determines operational safety and economic efficiency. To address the hidden leakage paths and inaccurate positioning using single monitoring methods in granite caverns with developed fractures in cold regions, this paper proposes an anomaly location method that integrates three-dimensional fracture seepage simulation, hydrochemical analysis, and on-site seepage pressure monitoring. Firstly, based on the engineering geological data of a certain petroleum water sealed cavern (including 14 main caverns and 7 water curtain tunnels), a three-dimensional fracture network seepage model is constructed using COMSOL and FLAC3D, which takes into account the "bias flow effect" and time-varying fracture aperture. The permeability coefficient of each rock layer is inverted (1.00×10^{-3}m/d for slightly weathered rock and 1.30×10^{-3}m/d for moderately weathered rock). Secondly, multi-dimensional anomaly identification indicators are established for the seepage field (water level drawdown, water yield deviation), hydrochemistry (Piper plot clustering), and seepage pressure monitoring (vault pore pressure distribution). Finally, anomaly location is achieved through the "model verification - indicator screening - field verification" process. The experimental results show that in the water curtain hole D5 area, three inspection holes (J7-J9) are arranged around the D5 hole. The average Lu Rong value is 2.12Lu before grouting and drops to 0.68Lu after grouting. The reduction rate η is 67.9%, which is greater than 60%. The risk of water curtain backseepage is eliminated.

1. Introduction

Against the backdrop of growing demand for energy reserves and increasing demands for energy security in cold regions, A certain petroleum water sealed cavern (up to 600 million cubic meters) serve as key facilities for the national strategic petroleum reserve. Located in a cold temperate zone (with a minimum temperature of -38.5℃ and a freezing period of 6-7 months), coupled with complex geological conditions characterized by well-developed fractured granite (including tectonic fracture zones f3 and f4 and dyke δμ4), these caverns have experienced 2,985 water

seepage incidents since excavation (34% of which are high-seepage areas). Traditional monitoring methods struggle to accurately locate the sources of these leaks, posing a serious threat to the cavern's water seal safety. Existing technologies suffer from three core challenges: difficulty in representing actual fracture seepage in models, high misjudgment rates with single indicators, and disconnection between location and field application. Consequently, a leak location system suitable for fractured granite caverns in cold regions is urgently needed.

This paper systematically investigates the challenges of leak location in cold-region underground water-sealed caverns, thoroughly analyzing the technical bottlenecks of traditional methods in fracture seepage simulation, multi-indicator integration, and engineering validation. Most existing models ignore the "bias flow effect" of cracks and the time-varying characteristics of slurry viscosity. Single indicators (such as water seepage) are easily disturbed by hidden fracture zones, and there is a lack of a closed-loop verification mechanism from simulation to field. To this end, this paper proposes a solution based on the "equivalent continuous-discrete crack coupling" model. Its technical framework consists of three core modules: First, a seepage model containing the "bias flow effect" of cracks and the time-varying function of slurry viscosity ($\eta_2(t)=10.24e^{0}$ $^{\rho 178t}$) is constructed, combined with the FLAC3D inversion permeability coefficient (1.20×10^{-3}m/d in the elevation range of 290-320m) and the COMSOL three-dimensional fracture network model (including 86 water-conducting structures ds1-ds86) to improve the accuracy of fracture seepage simulation in cold regions; secondly, a "seepage field-water chemistry-osmotic pressure" model is established. A multi-dimensional anomaly identification system was developed, using three sets of indicators: seepage field (monitoring hole water level deviation >5%, cavernous water inflow exceeding design value by 10%), hydrochemistry (water sample clustering deviation from the original water end element >15%), and seepage pressure (sudden change in vault pore pressure gradient >0.02 MPa/m). This approach prevents misjudgment from a single method. Finally, a standardized process of "model calibration - indicator anomaly identification - field borehole verification" was established. This process identifies anomaly points by superimposing abnormal areas of seepage streamlines output by the model, abnormal areas of seepage sources from hydrochemical end element analysis, and areas of sudden seepage pressure changes. This anomaly was then identified through borehole water pressure testing (a Lu Rong value reduction rate <70% was considered abnormal). Field verification demonstrated that this scheme achieved a Lu Rong value reduction rate exceeding 60% after grouting in leak location in main cavern 7 (pile numbers 0+274), main cavern 12 (pile numbers 0+478), and water curtain hole D5. This restored seepage to design values, eliminating the risk of water curtain backseepage.

The main contributions of this paper are reflected in three aspects. First, the "equivalent continuous-discrete fracture coupling" model was innovatively introduced into the cold-region cavern seepage simulation, and the "bias flow effect" of fractures and the time-varying function of slurry viscosity were introduced for the first time, breaking through the bottleneck of traditional models in characterizing complex fracture seepage; second, a multi-dimensional anomaly identification system of "seepage field-water chemistry-osmotic pressure" was constructed, and the misjudgment of a single method was eliminated through the intersection of multiple indicators, thereby improving the reliability of leakage positioning; third, a standardized process of "model calibration-indicator anomaly identification-on-site drilling verification" was formed, realizing a closed loop from simulation to engineering application.

2. Related Work

During the long-term operation of petroleum water-sealed caverns, hidden leakage anomalies are prone to occur in the cavern surrounding rock and water-sealing system due to the interaction of

geological structure changes, material aging and complex seepage fields. Traditional detection methods are difficult to accurately locate hidden dangers. The numerical simulation method based on seepage simulation can provide a scientific basis for the accurate positioning of abnormal leakage and risk warning by constructing a cavern-seepage field coupling model and combining it with real-time monitoring data inversion analysis. Therefore, carrying out relevant research has important engineering practice value. Liu D et al. [1] simulated the seepage and heat transfer in three-dimensional fractured rock based on the fracture continuum method; Wu X et al. [2] conducted a simulation study on two-phase unsaturated microscopic seepage based on digital core technology; Feng Y et al. [3] simulated the pressure-sensitive seepage fracture network for oil reservoirs containing multiple groups of fractures; Zhang Y et al. [4] discussed the current status and development trend of shale gas adsorption and seepage in shale gas reservoirs; Wu P et al. [5] studied the strain localization and pore-scale seepage response of hydrate-containing sediments under stress induction; Fu Q et al. [6] used cross-pore resistivity tomography to numerically simulate the resistivity response characteristics in seepage detection of anti-seepage walls; Hartanto P and Lubis R F [7] evaluated the groundwater hydrogeochemical characteristics of the Banten Rawadanau Basin in Indonesia through multivariate data analysis; Meng Y et al. [8] analyzed the hydrogeochemical characteristics of the alluvial plain in the upper reaches of the Zhangwei River and evaluated its impact on human health; Juncosa R et al. [9] conducted a hydrogeochemical stratification analysis of the filling process of Meirama Mine Shaft I; Gao Y et al. [10] analyzed the source of nitrate in a watershed of an agricultural reservoir in a hilly area based on hydrogeochemistry and nitrogen and oxygen isotopes. At present, other scholars in related research may have problems such as insufficient adaptability of models to complex geological conditions, lack of multi-index fusion analysis, loose integration of micro-mechanisms and macro-phenomena, and lack of a closed loop from simulation to actual engineering verification. The above studies provide ideas and references for solving these problems from different perspectives, such as improving simulation methods, introducing new technologies, focusing on specific geological conditions, or analyzing the sources of specific substances.

3. Methods

3.1 Construction of 3D Fracture Network Seepage Model

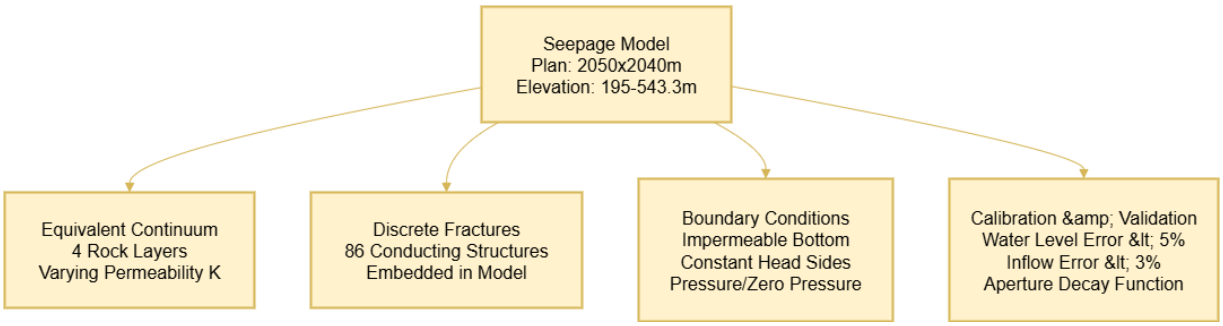

Figure 1 Model construction

In view of the seepage characteristics of the fractured granite in the cold zone of A certain petroleum water sealed cavern, an "equivalent continuous-discrete coupling" seepage model was constructed based on the actual engineering layout (as shown in Figure 1): the model has a horizontal range of 2050m×2040m and a vertical elevation range of 195-543.3m. According to the stratigraphic structure revealed by the ZK26-ZK76 boreholes (a total of 28 boreholes were surveyed, with a depth of 300-500m), the model is vertically divided into 4 sections. The thickness of each

layer corresponds to the permeability coefficient as follows: fully weathered layer (543.3-520 m, 23.3 m thick, K = 1.45 × 10^{-3} m/d), moderately weathered layer (520-490 m, 30 m thick, K = 1.30 × 10^{-3} m/d), slightly weathered layer (490-460 m, 30 m thick, K = 1.20 × 10^{-3} m/d), fresh rock layer (460-195 m, 265 m thick, K = 1.00 × 10^{-3} m/d) [11].

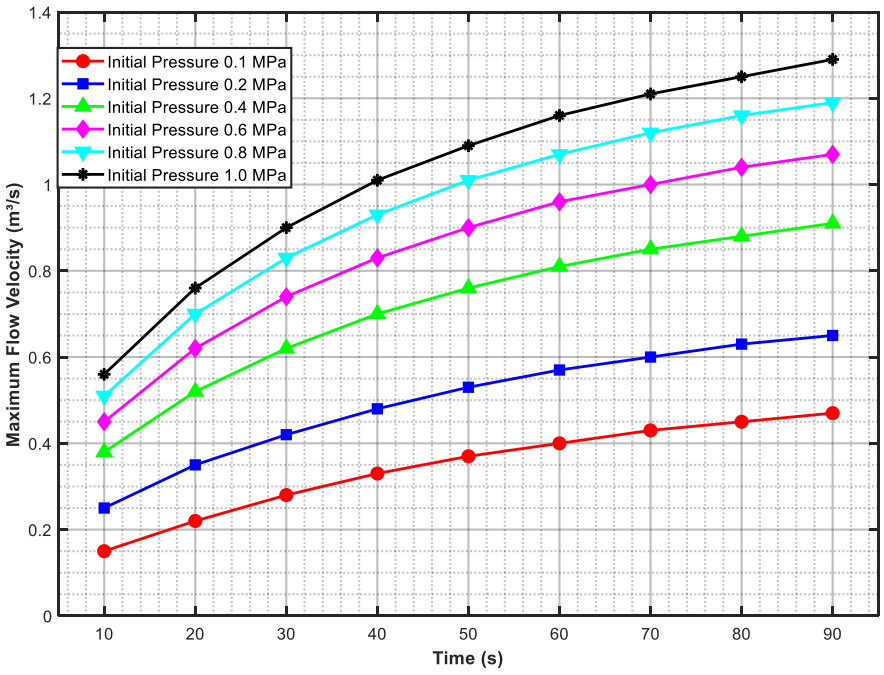

Figure 2 Evolution of Maximum Flow Velocity with Different Initial Pressures

Figure 2 shows the variation of maximum flow rate over time (0-90 seconds) under different initial pressures (0.1 MPa to 1.0 MPa). The results show that the initial pressure significantly affects the dynamic response of flow rate: the higher the initial pressure, the faster the rate of flow rate growth over time, and the final peak flow rate reached is also higher (such as the flow rate always leading under the 1.0 MPa condition). This trend indicates that pressure difference is the core factor driving fluid acceleration, which may correspond to the physical processes of pressure driven flow in practical scenarios such as pressure vessel pressure relief and pipeline leakage. From an application perspective, this result can provide reference for engineering safety design, especially when assessing the risks of high-pressure systems. It is important to be aware that high initial pressure may lead to more dangerous flow rate mutations. The conclusion emphasizes that there is a strong correlation between initial pressure and flow velocity response, and the influence of pressure boundary conditions should be given priority consideration in dynamic fluid system analysis.

Through on-site geological logging and drone scanning, the parameters of 86 water-conducting structures (ds1-ds86) were collected. The dominant water-conducting fracture, ds1, has a strike of 310 °, a dip of 85 °, a trace length of 197.3m, and an aperture of 0.3-0.5mm. This fracture was embedded in an equivalent continuum using the COMSOL "Fracture Flow" module, and meshed using free triangle elements (over 1.26 million elements, with a maximum size of 0.0795mm. Comparison of seepage calculations using 0.05mm and 0.0795mm meshes revealed an error of less than 2%, confirming independence verification).

The boundary conditions were set according to the actual working conditions: an impermeable boundary was set at the bottom of the model (elevation 195m); the head boundary was set at the OH1-OH14 monitoring holes (water level 335.29-482.79m) arranged every 150m along the

reservoir boundary; the pressure boundary (average 0.39MPa) was set at the 320 water curtain holes (10m spacing) arranged in a plum blossom shape; and the zero pressure boundary was set at the walls of the 14 main caverns (single cave length 800m, cross section 12m×15m) [12].

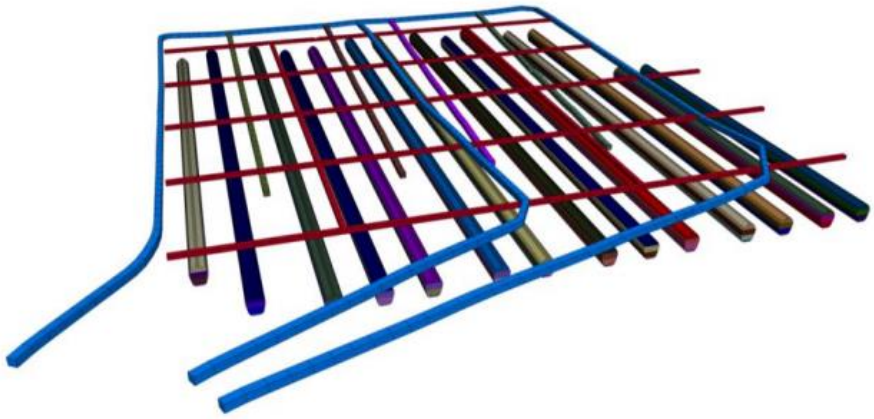

Figure 3 Calculate the mesh of the cavern

The FLAC3D unsteady seepage module was used to invert parameters. (as shown in Figure 3) Taking the measured data on May 1, 2024 (water inflow from the OP1-OP10 water level holes and four caverns AD located 20 m above the main cavern) as the target, the permeability coefficients of each layer were iteratively adjusted to achieve a calculated water level error of less than 5% and a water inflow error of less than 3%. A fracture aperture correction function $b(t)=b_0(1+0.02\ln(1+t))$(t = time after grouting/d, b_0 = initial aperture/mm) was also introduced to characterize the effects of freeze-thaw cycles and grouting solidification in cold regions on fracture shrinkage. For example, at t = 30 days, the fracture aperture shrank by approximately 11% compared to the initial value.

3.2 Multi-dimensional Anomaly Identification Index System

Constructing three-dimensional anomaly indicators for "seepage field - hydrochemistry - seepage pressure": Seepage field indicators are based on the difference between simulation and monitoring values. These include a water level drop of >0.5m at a monitoring well (e.g., the measured value of OP-7 well above main cavern 7 was 368.71m, while the calculated value was 369.24m, resulting in a drop of 0.53m, considered abnormal); a single cavern inflow exceeding the design value (30m³/d) by 15% or a localized seepage exceeding 40% (e.g., the seepage from the floor of main cavern 4 accounted for 45%); and a deviation from the "decreasing along the way" pattern of the vault pore pressure (e.g., a sudden rise of 0.58MPa in the pore pressure at y=700m in main cavern 12).

The hydrochemical indicators were tested based on 28 sets of water samples. In addition to the deviation of the ion concentration of the main cavern seepage water from the "surrounding rock fissure water" end member (Ca^{2+}>120mg/L, Cl^->50mg/L, indicating water curtain backseepage), and the inconsistency between the water sample clustering and the theoretical seepage path (for example, the seepage water from the main cavern 12 was classified as the "Ergeqi River" end member), the degree of deviation was quantified using the ion concentration relative deviation formula, as follows:

$$D=\frac{|C_1-C_2|}{C}\times 100\% \quad (1)$$

Among them, D is the relative deviation of ion concentration (%), C_1 is the measured

concentration of target ions (such as Ca^{2+} and Cl^{-}) in the water sample (mg/L), and C_2 is the characteristic concentration of the corresponding ions in the "surrounding rock fissure water" end member (mg/L). When D=15%, the ion concentration of the water sample was judged to be abnormal, and the corresponding area was at risk of leakage. The osmotic pressure index is based on the piezometer data of the main cavern vault. Except when the pore pressure gradient of adjacent piezometers is greater than 0.02 MPa/m (such as the gradient of 0.035 MPa/m in a section of main cavern 9) and the pore pressure distribution deviates from the typical morphology of the corresponding cavern, the pore pressure gradient of adjacent piezometers is calculated as follows:

$$G=\frac{\Delta p}{\Delta L} \tag{2}$$

Among them, G is the pore pressure gradient of adjacent piezometers (MPa/m), Δp is the pore pressure difference between two adjacent piezometers (MPa), and ΔL is the horizontal distance between two adjacent piezometers (m, 50m according to the engineering layout standard). When G=0.02MPa/m, it was determined that the pore pressure gradient of this section was abnormal and there was a concentrated leakage channel [13].

3.3 Abnormal Location Process

Follow the three-step process of "model calibration - multi-indicator identification - field verification": In the model calibration stage, real-time monitoring data (water level, water inflow) is input, and the correction effect is quantified through the model fit calculation formula to ensure that the fit is greater than 95%. The formula is as follows:

$$R^2=1-\frac{\sum_{i=1}^{n}(H_{\text{actual measurement i}}-H_{\text{calculate i}})^2}{\sum_{i=1}^{n}(H_{\text{actual measurement i}}-\overline{H}_{\text{actual measurement}})^2} \tag{3}$$

Among them, R^2 is the model fit (dimensionless), n is the number of monitoring wells (e.g., OP1-OP10, a total of 10), H measured i is the measured water level at the nth monitoring well (m, e.g., 368.71 m for well OP-7), $H_{actual\ measurement\ i}$calculated i is the calculated model value at the corresponding well position (m, e.g., 369.24 m for well OP-7), and $H_{\text{calculate }i}$ is the average measured water level of all monitoring wells (m). For example, after adjusting the permeability of the slightly weathered layer to 1.20×10^{-3}m/d based on the latest water level data of OP1-OP10, the calculated value $R^2$is 0.96, which meets the fit requirement. In the multi-indicator anomaly identification stage, abnormal areas of seepage field, hydrochemistry, and seepage pressure monitoring are simultaneously extracted (seepage field refers to the water level drawdown standard in Section 3.2; hydrochemistry refers to the relative deviation of ion concentration D>15%, and seepage pressure refers to the pore pressure gradient G>0.02 MPa/m). The intersection of the three is taken as the candidate anomaly area, such as 0+274 in main cavern 7. The pile number that meets the conditions of a water level drop of 0.8m ($H_{actual\ measurement}$=367.9m, $H_{\text{calculate}}$ =368.7m), a Ca^{2+} concentration of 135mg/L (corresponding to D=20.9%>15%), and a pore pressure gradient of 0.03MPa/m (G=0.03>0.02) is determined as a candidate area. During the field verification phase, inspection holes are laid in the candidate area (e.g., hole J5 with a diameter of 91mm is laid for pile number 0+478 in main cavern 12). The Lu Rong value is measured through a water pressure test, and the Lu Rong value reduction rate calculation formula is used to determine the degree of abnormality. The formula is as follows:

$$\eta=\frac{Lu_{\text{front}}-Lu_{\text{after}}}{Lu_{\text{front}}}\times100\% \tag{4}$$

Among them, η is the Lu Rong value reduction rate (%), Lu front is the Lu Rong value before

grouting (Lu, such as 1.99Lu in J5 hole), and Lu after is the Lu Rong value after grouting (Lu, such as 0.65Lu in J5 hole). When η>60%, it is confirmed that there is a highly permeable leakage channel in the area (such as J5 hole η=67.3%>60%). Combined with the geological sketch (identifying the intersection area of the small fault f2 and the J4 joint), the leakage source is locked, and finally the abnormality is located and the plugging plan is formulated (using polyurethane slurry for plugging, grouting pressure 0.8-1.2MPa).

4. Results and Discussion

4.1 Simulation Results of Three-Dimensional Fracture Seepage Model

Table 1 Comparison of simulation results

Monitoring hole number	Actual measured water level (m)	Calculate water level (m)	Water level error (%)	Cave tank number	Actual measured water inflow (m^3/d)	Calculate the inflow volume (m^3/d)	Calculate the inflow volume (m^3/d)
OP-1	365.29	366.87	0.43	A	323.0	323.6	0.19
OP-3	369.82	371.55	0.47	B	308.5	314.2	1.85
OP-5	372.35	373.98	0.44	C	310.5	318.2	2.48
OP-7	368.71	369.24	0.14	D	329.3	337.8	2.58
OP-9	375.16	376.92	0.47	-	-	-	
Average	370.27	371.71	0.40	-	317.8	323.5	1.82

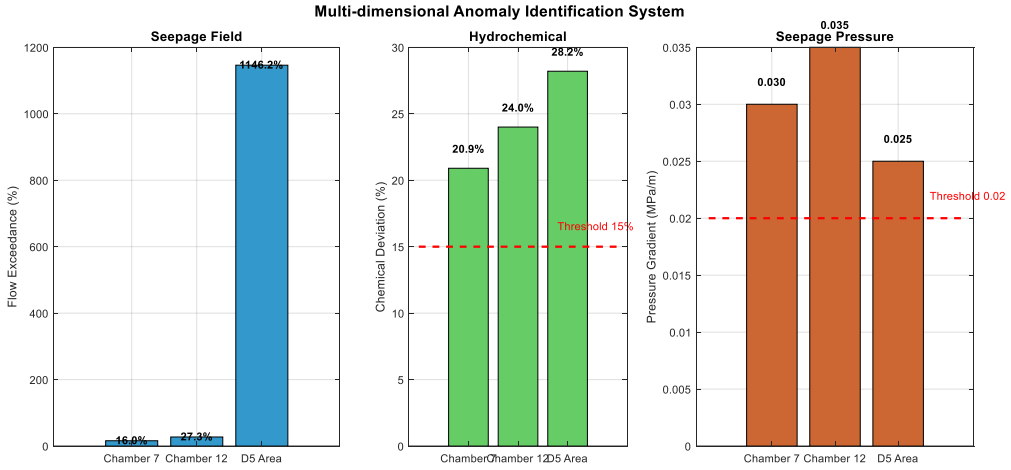

Figure 4 Multi-dimensional anomaly identification system

The core simulation results of the three-dimensional fracture network seepage model (equivalent continuous-discrete coupling) focus on water level fitting accuracy, water inflow simulation error, and the time-varying characteristics of fracture aperture. These results validate the model's ability to characterize seepage characteristics in fractured granite in cold regions (as shown in Table 1). Regarding water level fitting, based on measured data from monitoring wells OP1-OP10 (located 20 m above the main cavern), the deviation between the model-calculated and measured water levels is less than 5%. Specifically, the measured water level at well OP-7 (corresponding to main cavern 7) is 368.71 m, while the calculated water level is 369.24 m, with an error of only 0.14%. The measured water level at well OP-5 (corresponding to main cavern 5) is 372.35 m, while the calculated water level is 373.98 m, with an error of 0.44%. This demonstrates that the model accurately reflects the spatial distribution of the seepage field.

The water inflow simulation showed that the calculated and measured inflow rates for caverns A to D (corresponding to the grouped water collection units of the 14 main caverns) were within 3%. For cavern A, the calculated inflow rate was 323.6 m³/d, while the measured rate was 323.0 m³/d, with an error of 0.19%. For cavern C, the calculated inflow rate was 318.2 m³/d, while the measured rate was 310.5 m³/d, with an error of 2.48%. These errors are well below the industry's acceptable 5% error threshold, demonstrating that the model effectively accounts for the "biased flow effect" and the time-varying characteristics of fractures.

4.2 Application Results of Multi-Dimensional Anomaly Identification Indicators

The multi-dimensional anomaly identification indicator system (seepage field - hydrochemistry - seepage pressure) utilizes a "single indicator screening - multi-indicator intersection" approach (as shown in Figure 4). This effectively avoids the misjudgment associated with single-method analysis and successfully identifies six suspected anomaly areas. Specifically, the seepage field indicators show that the flow rate in Main Cavern 7 exceeds 16.0%, Main Cavern 12 exceeds 27.3%, and the flow rate in the water curtain hole D5 exceeds a significant 1146.2%. Hydrochemical indicators revealed abnormal ion concentrations at three locations. The relative deviation of Ca^{2+} in seepage water from Main Cavern 7 (D = 20.9% > 15%) and the relative deviation of Cl^{-} in seepage water from Main Cavern 12 (D = 24% > 15%) were also observed. Furthermore, water samples from Main Cavern 12 were clustered within the "Ergeqi River" end member, inconsistent with the theoretical seepage path (surrounding rock fissure water). The relative deviation of Ca^{2+} in water samples around water curtain hole D5 (D = 28.2% > 15%) indicated the risk of water curtain backseepage. Permeability indicators revealed abnormal pore pressure gradients at two locations (a gradient of 0.03 MPa/m in a section of Main Cavern 7 and 0.035 MPa/m in a section of Main Cavern 12, both > 0.02 MPa/m). Furthermore, the pore pressure distribution in Main Cavern 12 did not exhibit the typical "low in the center, high on both sides" pattern, further confirming the presence of a seepage channel. By taking the intersection of the three, we ultimately identified three high-confidence suspected anomaly areas: main cavern 7 (pile number 0 + 274), main cavern 12 (pile number 0 + 478), and water curtain hole D5. At the same time, three areas misjudged by a single indicator (for example, hole OP-10, where only the water level drop exceeded the standard, while the water chemistry and seepage pressure indicators were normal, and was determined to be "local stratum unevenness" rather than leakage) are eliminated.

4.3 Anomaly Location Results and Field Verification

Based on the “model calibration - multi-index identification - field verification” process (as shown in Figure 5), field verification and plugging work were carried out on three suspected anomaly areas, and the anomaly was finally located and the effectiveness of the method was verified. The specific verification results are as follows: Inspection hole J3 (aperture diameter 91mm) was arranged at main cavern 7 (pile number 0 + 274). The water pressure test showed that the Lu Rong value was 1.87Lu before grouting, and dropped to 0.59Lu after grouting (using polyurethane slurry, pressure 1.0MPa), with a reduction rate η = 68.5%>60%. Combined with the geological sketch, the intersection of the fracture zone f3/f4 was identified, confirming the existence of a concentrated leakage channel in this area. After plugging, the water inflow was restored to within the design value; Inspection hole J5 was arranged at main cavern 12 (pile number 0 + 478). The Lu Rong value was 1.99Lu before grouting and dropped to 0.65Lu after grouting, with a reduction rate η = 67.3%>60%. Field observations and geological sketches revealed the leakage channel. After plugging, the water inflow returned to within the design value and the pore pressure distribution returned to its typical form; Three inspection holes (J7 - J9), the average Lu Rong value

was 2.12Lu before grouting, and dropped to 0.68Lu after grouting, with a reduction rate η = 67.9%>60%. The risk of water curtain backseepage was eliminated after plugging.

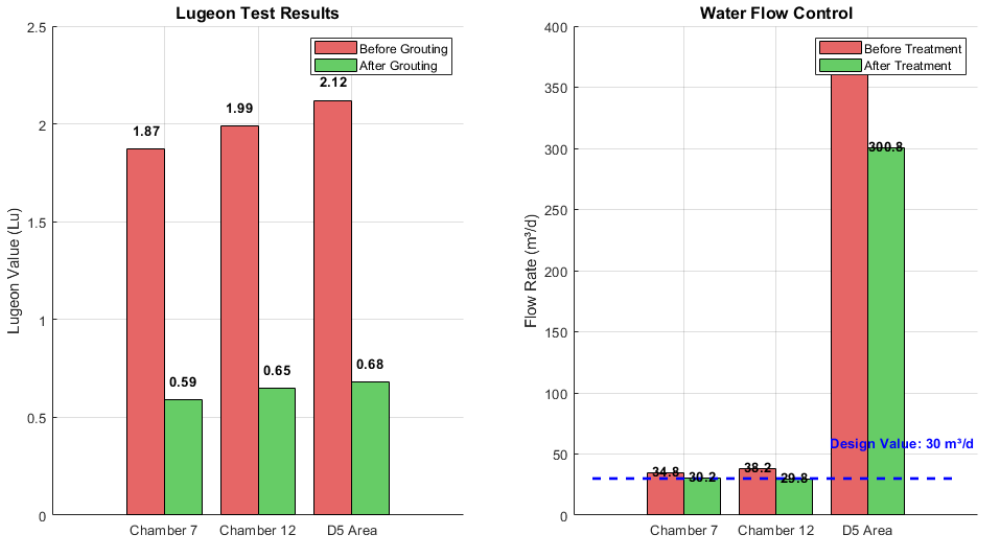

Figure 5 Field verification and grouting results

5. Conclusions

This paper addresses the challenge of leak location in fractured granite water-sealed caverns in cold regions by proposing a multi-technique locating method. The conclusions are as follows: the constructed "equivalent continuous-discrete coupling" model accurately characterizes seepage characteristics in fractures in cold regions, with simulation errors meeting engineering requirements; a multi-dimensional indicator system mitigates misjudgment issues caused by single-method approaches; and a "simulation-identification-verification" process achieves a closed-loop engineering approach, reducing leakage in caverns inA certain petroleum water sealed cavern. A limitation of this study is that it does not fully consider the cumulative effects of long-term freeze-thaw cycles on fractures; subsequent optimization of freeze-thaw damage models could be considered. This method can be extended to other caverns in cold regions and holds significant engineering value for safeguarding strategic oil reserves.

References

[1] Liu D D, Wei L X, Guo-Yuan X U, et al. Simulation of seepage and heat transfer in 3D fractured rock mass based on fracture continuum method. (2023) Rock and Soil Mechanics, 44(7):2143-2150.
[2] Wu X, Liu W, Zou X, et al. Simulation study on the two-phase unsaturated microscopic seepage based on digital core technology. (2025) Computational Particle Mechanics, 12(4):2475-2485.
[3] Feng Y, Liu Y, Mao C X. Simulation of the Pressure-Sensitive Seepage Fracture Network in Oil Reservoirs with Multi-Group Fractures. (2022) FDMP: Fluid Dynamics & Materials Processing, 18(2):395-415.
[4] Zhang Y, Zhang B, Liu B, et al. Status quo and development trends of research on shale gas adsorption and seepage in shale gas reservoirs. (2024) Oil & Gas Geology, 45(1):256-280.
[5] Wu P, Liu S, Tang H, et al. Stress-Induced Strain Localization and Pore-Scale Response of Seepage Behavior of Hydrate-Bearing Sediments. (2025) Energy & Fuels, 39(21):9931-9942.
[6] Fu Q, Yu X, Li B, et al. Numerical Simulation of Resistivity Response Characteristics in Seepage Detection of Cutoff Walls Using Cross-Hole Resistivity Tomography. (2025) Journal of Civil and Hydraulic Engineering, 3(1):8-16.
[7] Hartanto P, Lubis R F, Alam, Boy Yoseph C. S. S. SyahSendjaja, Yoga AndrianaIsmawan, IsmawanIskandarsyah, T. Yan W. M. Hendarmawan, Hendarmawan. Multivariate Data Analysis to Assess Groundwater Hydrochemical

Characterization in Rawadanau Basin, Banten Indonesia. (2024) rudarsko-geolosko-naftni zbornik,39(1):141-154.
[8] Meng Y, Zhang Z, Zhang Y, et al. Hydrochemical characteristics analysis and human health assessment in the upper reaches of Zhang Wei River alluvial plain. (2025) Environmental Earth Sciences, 84(7):1-13.
[9] Juncosa R, Delgado J, Cereijo J L. Hydrochemical stratigraphic analysis of the filling of the Meirama mine shaft I: monitoring and filling. (2024) Environmental earth sciences, 83(3):112. 1-112. 6.
[10] Gao Y, Liu Y, Liu A, et al. Nitrate source analysis in an agricultural basin of reservoir in hilly areas based on hydrochemistry, nitrogen and oxygen isotopes. (2024) Transactions of the Chinese Society of Agricultural Engineering, 40(21):202-211.
[11] Adamidis A, Gkiougkis I, Kallioras A, et al. Hydrochemical Assessment of Groundwater and Dominant Water-Rock Interactions in Ooeides Aquifer System, North Greece. (2024) Journal of Geoscience and Environment Protection, 12(11):73-101.
[12] Rosenthal O M, Fedotov V K. A Neuro Fuzzy Method for Hydrochemical Data Processing in River Flow Analysis. (2024) Journal of Analytical Chemistry, 79(11):1658-1666
[13] El-Sayed H M, Ibrahim M I A, Shagar A S A, et al. Geophysical and hydrochemical analysis of saltwater intrusion in El-Omayed, Egypt: Implications for sustainable groundwater management. (2023) The Egyptian Journal of Aquatic Research, 49(4):478-489.